atmosphere

MDPI

Article

Characteristics and Driving Mechanisms of Coastal Wind Speed during the Typhoon Season: A Case Study of Typhoon Lekima

Lingzi Wang [1], Aodi Fu [2], Bashar Bashir [3], Jinjun Gu [2], Haibo Sheng [1], Liyuan Deng [1], Weisi Deng [1] and Karam Alsafadi [4,*]

[1] Power Dispatching and Control Center of China Southern Power Grid, Guangzhou 510663, China; wanglz2@csg.cn (L.W.); dengly3@csg.cn (L.D.)
[2] School of Geographical Sciences, Nanjing University of Information Science & Technology, Nanjing 210044, China
[3] Department of Civil Engineering, College of Engineering, King Saud University, P.O. Box 800, Riyadh 11421, Saudi Arabia
[4] Key Laboratory of the Ministry of Education for Coastal and Wetland Ecosystems, College of Environment and Ecology, Xiamen University, Xiamen 361102, China
* Correspondence: karam.alsafadi@xmu.edu.cn

Abstract: The development and utilization of wind energy is of great significance to the sustainable development of China's economy and the realization of the "dual carbon" goal. Under typhoon conditions, the randomness and volatility of wind speed significantly impact the energy efficiency and design of wind turbines. This paper analyzed the changes in wind speed and direction using the BFAST method and Hurst index based on data collected at 10 m, 30 m, 50 m, and 70 m heights from a wind power tower in Yancheng, Jiangsu Province. Furthermore, the paper examined the causes of wind speed and direction changes using wind speed near the typhoon center, distance from the typhoon center to the wind tower, topographic data, and mesoscale system wind direction data. The conclusions drawn are as follows: (i) Using the BEAST method, change points were identified at 10 m, 30 m, 50 m, and 70 m heights, with 5, 5, 6, and 6 change points respectively. The change points at 10 m, 30 m, and 50 m occurred around node 325, while the change time at 70 m was inconsistent with other heights. Hurst index results indicated stronger inconsistency at 70 m altitude compared to other altitudes. (ii) By analyzing the wind direction sequence at 10 m, 30 m, 50 m, and 70 m, it was found that the wind direction changes follow the sequence Southeast (SE)—East (E)—Southeast (SE)—Southwest (SW)—West (W)—Northwest (NW). Notably, the trend of wind direction at 70 m significantly differed from other altitudes during the wind speed strengthening and weakening stages. (iii) Wind speed at 10 m and 70 m altitudes responded differently to the distance from the typhoon center and the wind near the typhoon center. The correlation between wind speed and the distance to the typhoon center was stronger at 10 m than at 70 m. The surface type and the mesoscale system's wind direction also influenced the wind speed and direction. This study provides methods and theoretical support for analyzing short-term wind speed changes during typhoons, offering reliable support for selecting wind power forecast indicators and designing wind turbines under extreme gale weather conditions.

Keywords: BEAST; Hurst index; Typhoon Lekima; wind speed characteristics; driving mechanism

Citation: Wang, L.; Fu, A.; Bashir, B.; Gu, J.; Sheng, H.; Deng, L.; Deng, W.; Alsafadi, K. Characteristics and Driving Mechanisms of Coastal Wind Speed during the Typhoon Season: A Case Study of Typhoon Lekima. *Atmosphere* **2024**, *15*, 880. https://doi.org/10.3390/atmos15080880

Academic Editors: Anthony R. Lupo and Leonardo Primavera

Received: 9 May 2024
Revised: 4 July 2024
Accepted: 13 July 2024
Published: 24 July 2024

1. Introduction

Wind is one of the renewable resources, and the rational development and utilization of wind energy are of great significance to the sustainable development of China's economy and the realization of the "double carbon" goal [1]. Due to the influence of weather systems such as underlying surface characteristics, air temperature, atmospheric pressure, and global circulation patterns, wind speed is characterized by randomness and fluctuation in a short period, which causes the power generation of wind turbines to fluctuate and affects

the stability of the power grid [2]. Additionally, the fluctuation of wind speed imposes higher requirements on the fatigue resistance of the main mechanical components of wind turbines [3]. Typhoons, as the main weather system that affects the working status of wind turbines, impose higher requirements for the design and selection of wind turbines. Analyzing the non-stationarity characteristics of wind speed around wind farms and its influencing factors during typhoon transit is of far-reaching significance for the refined prediction of wind power and the design of wind turbine components [4].

The non-stationarity of wind speed refers to the periodicity and fluctuation of wind speed on different time scales due to the influence of weather systems such as underlying surface characteristics, temperature, atmospheric pressure, and various circulation patterns [5–8]. Chen et al. utilized daily sounding wind data from Wuhan spanning from 1958 to 2013 to analyze the non-stationarity characteristics of annual, seasonal, and monthly mean wind speeds using deviation coefficient, climate tendency rate, wavelet analysis, Yamamoto mutation test, and other methods [9]. Drawing from the 1971–2015 average wind speed data of 155 meteorological stations in northern China, Han Liu et al. employed climate trend analysis, spatial interpolation, and wavelet analysis to examine the annual and seasonal spatio-temporal variation trends and periodic characteristics of the wind erosion area in northern China [10]. Understanding long-term wind change characteristics can provide early technical support for regional wind resource assessment, wind farm location, and design [11,12].

Presently, an increasing number of studies focus on short-term wind characteristics. For instance, Chen Wenchao et al. [13] utilized observation data from the 80 m meteorological tower in Dongguan, China during Typhoon "Molave", strong convection, and strong cold air events. They compared and analyzed the characteristics of average wind direction, power index of wind profile, turbulence intensity, wind attack angle, turbulence spatial integral scale, and turbulence power spectrum. Similarly, Wang Hailong et al. [14] analyzed the time–history variation characteristics of wind shear index, turbulence intensity, gust factor, and wind direction before and after super Typhoon "Rammasun" (No. 1409) made landfall in Xuwen, Guangdong, using observation data from the Warrior Wind Farm during Rammasun's landing. The study of short-term strong wind characteristics provides a theoretical basis for transmission line design, selection, and wind turbine design [15].

In the non-stationary detection of short-term wind speed, researchers often utilize linear methods such as time series parametric and non-parametric tests, including the Mann–Kendall (MK) test, which can merely describe the trend characteristics of time series [16]. During the period of typhoon transit, wind speed is often characterized by strong volatility. Currently, the primary methods employed to detect the non-stationarity and nonlinearity of time series changes include Empirical Mode Decomposition (EMD) [17], Detecting Breakpoints and Estimating Segments in Trend (DBEST) [18], the Breaks for Additive Season and Trend Monitor (BFAST) [19], and Bayesian Estimator of Abrupt change, Seasonal change, and Trend (BEAST) [20].

EMD is an adaptive signal processing method that explores local time characteristics and can address the non-stationarity trend of time series. However, when all extreme value points are included, noise increases EMD error, leading to distortion of prediction results [17]. DBEST can rapidly and reliably detect breakpoints in time series changes and accurately estimate the time and amplitude of changes, although it cannot identify changes in the period of time series [21]. BFAST can identify long-term trends and breakpoint changes in time series, elucidating the periodic components. Similarly, BEAST can also identify long-term trends and breakpoint changes in time series, with higher accuracy in detecting breakpoint information compared to BFAST [20]. BEAST finds widespread application in detecting surface vegetation, climate change, and social-ecological indicators, among others [22]. The Hurst index is frequently employed to analyze the long-term correlation and self-similarity of wind speed in time series [23]. Xu et al. utilized the Hurst index to analyze the time series of wind speed per minute in 2017 from a wind tower in the United States Wind Energy Research Center. Their findings revealed sharp fluctuations in

wind speed and irregular monthly wind speed fluctuations, suggesting strong nonlinear characteristics [24].

Previous researchers have predominantly focused on studying the changing characteristics of wind speed, wind direction, and path during typhoons, as well as the temperature and precipitation caused by these storms. For instance, Cai et al. [25] analyzed the turbulent characteristics of Typhoon "Lekima" during its transit based on the 10-min average wind speed and direction data from the Cixi Observation Station. Similarly, Sun et al. [26] analyzed the atmospheric pressure field reanalysis data of ERA5 to elucidate the precipitation mechanism in Shandong triggered by "Lekima". However, the development mechanism of the changing characteristics of wind speed during typhoons remains unexplored.

Studying the non-stationarity of wind speed and its influencing factors is crucial for wind power system modeling and the timely and accurate prediction of wind power. This paper addressed these issues by utilizing 15-min wind speed and direction data from a coastal wind farm in Dafeng District, Yancheng, Jiangsu Province. The BEAST method and Hurst index analysis were applied, along with typhoon track data, surface data, and mesoscale meteorological system data, to address the following objectives:

(i) Analyzing the non-stationarity characteristics of wind speed at the measuring tower during typhoon transit using the BEAST method and Hurst index;
(ii) Investigating the causes of wind speed non-stationarity by considering factors such as wind tower wind direction, the distance between the typhoon center and the wind tower, the wind level near the typhoon center, the characteristics of the surface under the typhoon's path, and the meridional and zonal wind speed characteristics of mesoscale systems.

The remainder of this paper is organized as follows: Section 2 describes the methodology, followed by an overview of Typhoon "Lekima" and its data sources in Section 3. Sections 4 and 5 present and discuss the research results in detail, and finally, Section 6 provides the conclusions.

2. Methodology

2.1. BEAST Method for Mutation Detection

BEAST is a method introduced by Zhao Kaigang in 2019 for detecting change points in time series, commonly applied in detecting changes in surface conditions, climate patterns, river runoff, etc. This method employs Bayesian probability prediction, dividing the time series into three segments: seasonal signal, trend signal, and abrupt change point. The calculation formula is outlined as follows [20]:

$$\hat{y}(t_i) = f(t_i; \ominus) = S(t_i; \ominus_S) + T(t_i; \ominus_T), i = 1 \cdots, n. \quad (1)$$

where $\ominus_S$ and $\ominus_T$ represent seasonal and trend signals; t is a time series.

2.2. Hurst Stationarity Analysis of Time Series

The Hurst index formula is calculated using the R/S method as follows [24,27]:

(1) A time series of length N $(P(t))$ $P_{k,a}$ divide A consecutive non-overlapping subintervals of n growth $I_a (a = 1, 2, \cdots, A)$, Each element of I_a is $P_{k,a} (k = 1, 2, \cdots, n)$;
(2) For each subinterval, calculate its standard deviation S_i, cumulative mean deviation $X_{k,a}$, and range R_i respectively:

$$S_i = \sqrt{\frac{1}{n}\sum_{k=1}^{n}(P_{k,a} - e_a)^2} \quad (2)$$

$$x_{k,a} = \sum_{i=1}^{k}(P_{i,a} - e_a) \quad (3)$$

$$R_i = \max_{1 \le k \le n} \left(x_{k,a} \right) - \min_{1 \le k \le n} \left(x_{k,a} \right) \quad (4)$$

where, e_a is the mean of the I_a sequence.

(3) Calculate the (R/S) of each subinterval and the average $(R/S)_n$ of "A" interval _n:

$$(R/S)_n = \frac{1}{A} \sum_{a=1}^{A} (R/S) \quad (5)$$

(4) Change the subinterval in step (1) and repeat step (1)–(3) to calculate the range value for different subinterval lengths $(R/S)_n$ $\lg(R/S)_n$ and lgn there is a linear relationship, that is,

$$\lg\left(\left(\frac{R}{S} \right)_n \right) = \lg\theta + H\lg n. \quad (6)$$

The average range and subinterval length are plotted on the log-log coordinate plot, and the slope H is the Hurst index through linear fitting by the least squares method.

The Hurst index quantitatively describes the long-term correlation. When $0 < H < 0.5$, it means that the event sequence is a long-term negative correlation, that is, if the time series shows an increasing trend in a certain interval, the following intervals are likely to decrease, and vice versa. When $H \approx 0.5$, it indicates that the time series has no long-term correlation and belongs to a non-autocorrelation random process similar to "white noise". When $0.5 < H < 1$, it means that the time series is positively correlated in the long run, that is, if the time series is growing in one interval, the next interval may also grow, and vice versa.

3. Overview of Typhoon Likima and Its Data Sources

3.1. Overview of Typhoon Lekima

Super Typhoon Lekima (2019) is the fifth strongest typhoon to make landfall in mainland China since 1949 [28]. On 4 August 2019, Typhoon "Lekima" (No. 201909) intensified into a tropical storm in the northwest Pacific Ocean (Figure 1). Between 4 August and 10 August, it swiftly moved northwestward, traversing the East China Sea, and made landfall in Wenling City, Zhejiang Province, China, as a super typhoon on 10 August, boasting a central wind speed of 52 m/s [29]. Subsequently, it continued northward and reached Dafeng District, Yancheng City, Jiangsu Province, passing through at 7:00 on 11 August. During this time, the maximum wind speeds measured by the wind tower of a coastal wind farm in Dafeng District were 23 m/s, 24 m/s, 25 m/s, and 19 m/s at 10 m, 30 m, 50 m, and 70 m heights, respectively, over a 15-min interval. The typhoon ultimately dissipated at 11:00 on 13 August 2019, in the Bohai Sea, China.

3.2. Data Source

In this study, wind speed and wind direction data were obtained from a cup anemometer with a sampling frequency of times/15 min installed on a wind tower (120.7° E, 33.3° N) at a coastal wind farm in Yancheng City, Jiangsu Province. The data at the heights of 10 m, 30 m, 50 m, and 70 m were obtained using linear interpolation. Missing values in the time series were interpolated using linear interpolation, and the time series was smoothed using a moving average technique, resulting in a complete time series of 672 data points. Typhoon path data were obtained from the Typhoon Path Network (https://typhoon.slt.zj.gov.cn/, accessed on 1 August 2023), encompassing the position of the typhoon center, near-center air pressure, wind scale data, and the calculated distance between the wind tower and the typhoon center using ArcGIS 10.2 neighborhood analysis tools. ASTER GDEM 30 m surface elevation data were retrieved from the Geospatial Data Cloud Platform (https://www.gscloud.cn, accessed on 12 November 2023). Additionally, 30 m resolution land use/cover data for 2019 were downloaded from the National Cryosphere Desert Data Center (https://www.ncdc.ac.cn/portal/metadata/9de270f3-b5ad-4e19-afc0-2531f3977f2f, accessed on 12 November 2023). The DEM and land use data were processed through

clipping and mosaic procedures to generate a terrain and surface-type map of the region traversed by the typhoon. Furthermore, wind direction data for the mesoscale system (zonal wind U and meridional wind V) underwent reanalysis using the NCEP/DOE Reanalysis II dataset. This dataset was acquired from the US National Oceanic and Atmospheric Administration (NOAA) Physical Science Laboratory (PSL) website (https://psl.noaa.gov/data/gridded/data.ncep.reanalysis2.html, accessed on 3 January 2024).

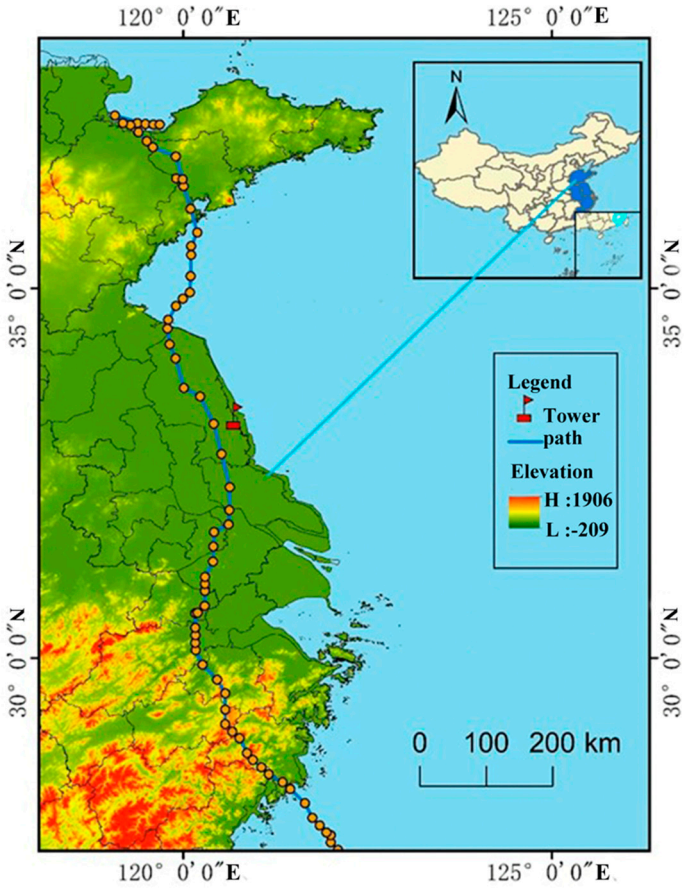

Figure 1. Overview of Typhoon Lekima.

4. Results

The BEAST method is used to detect breakpoint information in the time series, determining the start and end times of the typhoon's influence on the wind tower. It also analyzes the change characteristics of the time series at different stages during the typhoon's influence. In this study, the maximum number of trend change points (Mtcp) was set to 10, and the minimum separation interval (htcp) was set to 96. The detection signal at the heights of 10 m, 30 m, 50 m, and 70 m showed good correlation with the true value, with correlation coefficients of 0.99, 0.99, 0.98, and 0.96, respectively.

4.1. Characteristics of Wind Speed Change of Measuring Tower during Typhoon Influence Phase

4.1.1. Breakpoint Analysis of Wind Speed Sequence of Measuring Tower during Typhoon Influence Phase

Based on the influence range of the typhoon track and geopotential height, this paper performed a breakpoint analysis of the wind speed sequence during the typhoon's influence phase. At this stage, the BEAST method was adopted to detect the number of change points in the wind speed time series at 10 m, 30 m, 50 m, and 70 m of the wind tower, which were found to be 5, 5, 6, and 6, respectively, as shown in Figure 2. The probability values of all breakpoints were maintained above 0.52. The change point information for the 10 m height was at 324, 76, 154, 598, and 407; for the 30 m height at 325, 76, 402, 155, and 598; for the

50 m height at 324, 249, 428, 154, 554, and 478; and for the 70 m height at 306, 371, 554, 160, 429, and 56.

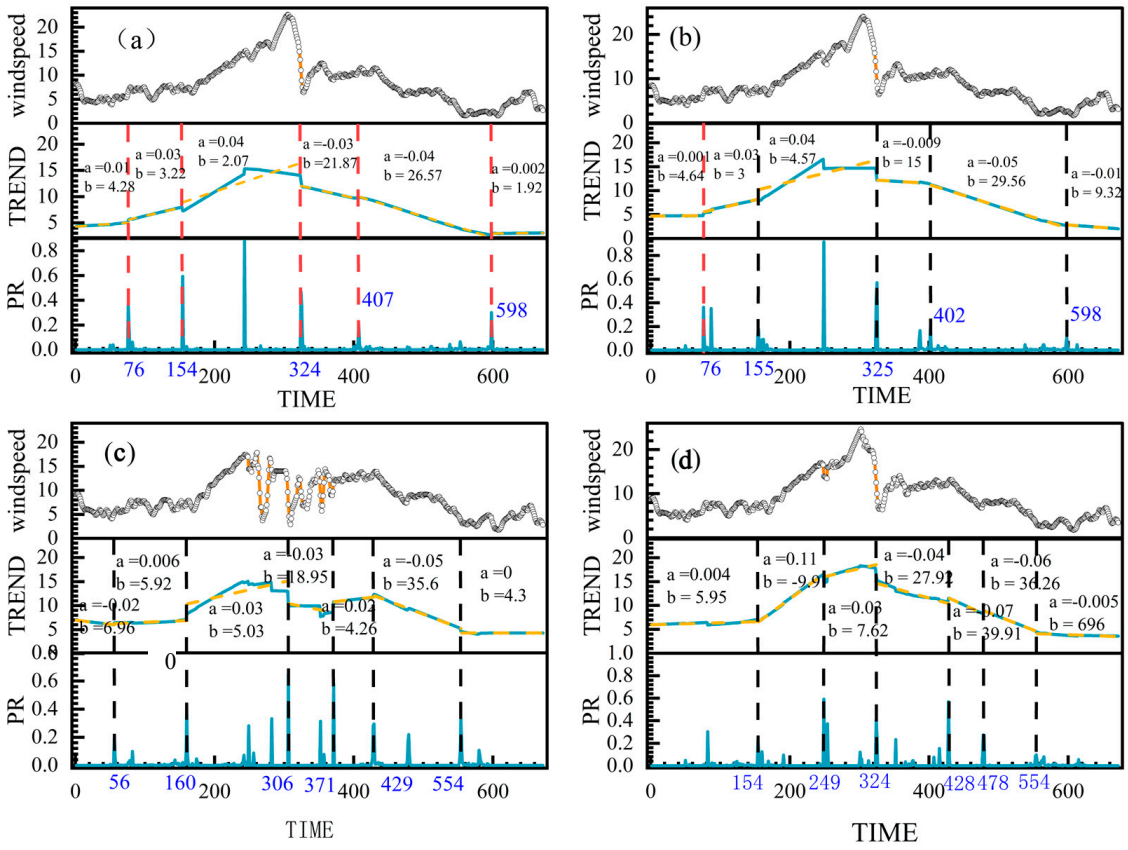

Figure 2. Beast method breakpoint detection (**a**–**d**).

This indicates that the airflow field changes rapidly before and after the typhoon passes, weakening the stationarity of the wind speed series. Except for the wind speed sequence at 70 m height, abrupt change points appeared at 154, 324, and 598 points at 10 m, 30 m, and 50 m altitudes. This suggests that the period during which the typhoon significantly impacted the wind tower was from point 154 to 598. At 70 m altitude, abrupt change points were observed at 56, 306, and 371, which may be due to the greater distance from the underlying surface. The roughness of the underlying surface has little influence at this height.

4.1.2. Analysis of Series Trend of Wind Speed of Measuring Tower during Typhoon Influence Stage

As can be seen from Table 1, based on the slope of the time series before and after abrupt points, except for the tower at 70 m height, the sequence can be roughly divided into two stages: intensification stage—weakening stage and strengthening stage time series. Meanwhile, the wind speed time series at 70 m height can be divided into four stages: intensification—weakening—intensification—weakening. At 10 m height, the slope changes were 0.01, 0.03, 0.04, 0.03, 0.04, and 0.002. At 30 m height, the slope changes were 0.001, 0.03, 0.04, 0.009, 0.05, and 0.01. The slope changes at 50 m height were 0.004, 0.11, 0.03, 0.04, 0.07, 0.06, and 0.005. At 70 m height, the slope changes were 0.02, 0.006, 0.03, 0.03, 0.02, 0.05, and 0. It can be observed that wind speed at 70 m altitude shows a stronger lag in response to the typhoon, indicating less smooth airflow.

Table 1. Beast point in time and probability value at the breakpoint.

Cp10	Time10	Pr10	Cp30	Time30	Pr30	Cp50	Time50	Pr50	Cp700	Time70	Pr70
76	2019/8/8 18:45	0.8	76	2019/8/8 18:45	0.98	154	2019/8/9 14:15	0.81	56	2019/8/8 13:45	0.52
154	2019/8/9 14:15	0.77	155	2019/8/9 14:30	0.69	249	2019/8/10 14:00	1	160	2019/8/9 15:45	0.95
324	2019/8/11 8:45	0.99	325	2019/8/11 9:00	1	324	2019/8/11 8:45	1	306	2019/8/11 4:15	1
407	2019/8/12 10:00	0.62	402	2019/8/12 4:00	0.85	428	2019/8/12 10:45	0.95	371	2019/8/11 20:30	1
598	2019/8/12 5:30	0.72	598	2019/8/12 5:30	0.59	478	2019/8/12 23:15	0.7	429	2019/8/12 11:00	0.87
						554	2019/8/13 18:15	0.7	554	2019/8/13 18:15	1

4.2. Hurst Index Analysis

In summary, the wind speed time series can be segmented into two distinct stages: the strengthening stage and the weakening stage. The Hurst index is utilized to assess the smoothness of these two time series. Specifically, the strengthening stage spans from data points 76 to 325, while the weakening stage encompasses data points 326 to 598. Based on this segmentation, the Hurst index was calculated for both stages, as illustrated in Figure 3.

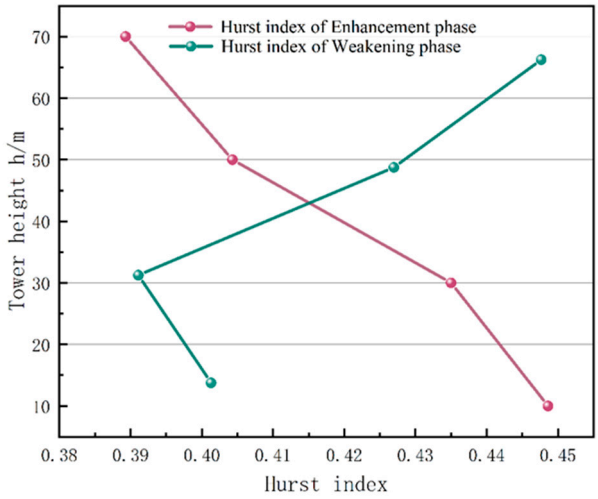

Figure 3. Hurst index calculation results.

During the intensification stage, the Hurst index ranges from 0.38 to 0.45, with goodness of fit R^2 values ranging from 0.88 to 0.94 across different heights of the wind measurement tower. Conversely, during the weakening stage, the Hurst index ranges from 0.36 to 0.4, with goodness of fit R^2 values ranging from 0.7 to 0.84. These results suggest that when the typhoon is active, the wind speed exhibits a Hurst index ranging from 0.38 to 0.45, with goodness of fit R^2 values between 0.8 and 0.94.

Furthermore, both the intensification and weakening stages of the wind speed time series demonstrated a pronounced long-term negative correlation. A comparison between the strengthening and weakening stages reveals that the Hurst index tended to decrease with the increasing height of the wind measurement tower during the strengthening stage. Conversely, during the weakening stage, the Hurst index generally increased with height. This indicates that the self-similarity of wind speed increases with height during the strengthening stage, while it decreases with height during the weakening stage. These trends may be attributed to variations in the airflow field before and after the passage of the typhoon.

4.3. Analysis of Wind Direction Change Characteristics

Based on the intensification and weakening stages, the alterations in wind direction were scrutinized. As illustrated in Figure 4, throughout the duration when the measuring tower experienced the typhoon's influence, the wind direction exhibited a sequence of shifts from southeast (SE) to east (E), southeast (SE), south (S), southwest (SW), west (W), and northwest (NW). The average magnitude of these directional changes across all four altitudes was 233°, indicating Typhoon Lekima was within the vigorous wind zone of the eyewall.

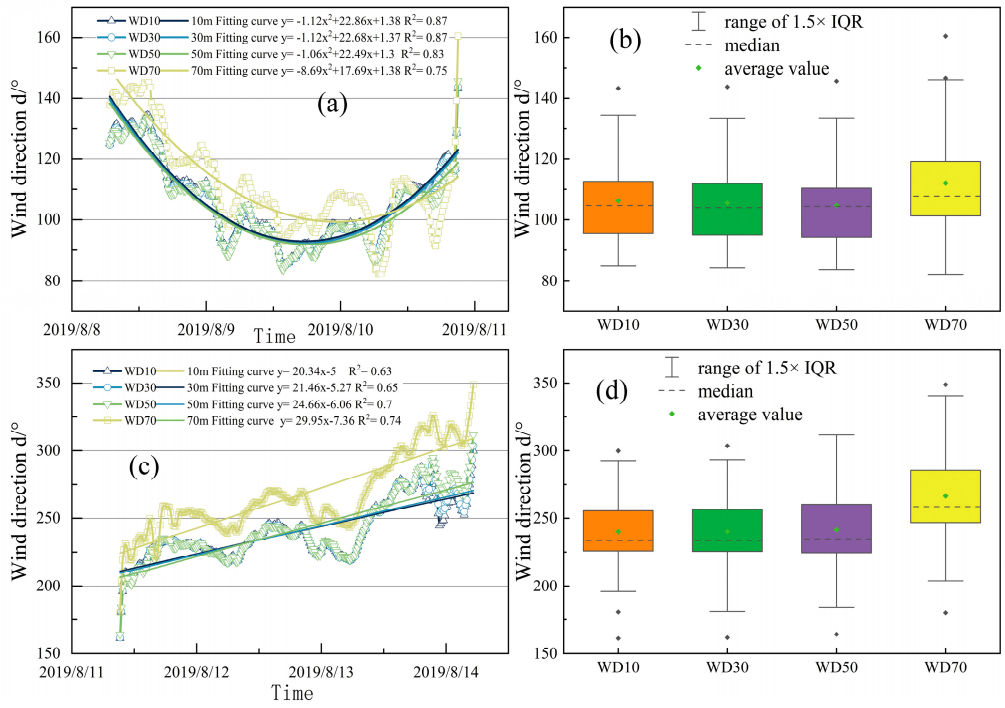

Figure 4. Wind direction variation characteristics during intensification and weakening phases, where, (**a**) is the wind direction during the wind speed increasing period, (**b**) is the statistical value of wind direction during the wind speed increasing period, (**c**) is the wind direction during the wind speed weakening period, and (**d**) is the statistical value of wind direction during the wind speed weakening period.

During the intensification stage, the wind speed time series was fitted with a quadratic polynomial, yielding R^2 values exceeding 0.75 across various heights of the wind tower. Conversely, a linear fit was employed for the wind speed time series during the weakening stage, resulting in R^2 values surpassing 0.63 at different tower heights. The higher R2 values in both stages suggest a strong fitting performance.

In the intensification stage, the wind direction transitioned from southeast to east before reverting back to southeast. The fitting curves of the wind speed series at 10 m, 30 m, and 50 m heights exhibited a high level of consistency, whereas the wind speed series curve at 70 m altitude showed a distinct trend. Prior to 20 August 2019, the wind speed series curve at 70 m altitude exceeded those of other altitudes, but after this point, it fell below them. Concurrently, during the weakening stage, the wind direction swiftly shifted from southeast to southwest and ultimately to northwest. Notably, the wind direction series at 70 m altitude displayed a persistently higher trend of directional change, particularly around 9 November 2019, indicating sharp alterations in the airflow field surrounding the measurement tower before and after midnight when the typhoon passed through. Statistical analysis of wind direction during the intensification and weakening stages revealed that the mean and median wind directions at the 70 m height were higher than those at other altitudes. Conversely, wind direction statistics at other altitudes exhibited similar values.

This suggests that wind direction at 70 m height is less influenced by underlying surface conditions and more affected by the circulation patterns of the typhoon.

4.4. Relationship between Wind Speed Variation Characteristics and Paths at 10 m and 70 m

As depicted in Figure 5, the relationship between central pressure and wind speed near the typhoon center is inversely proportional: the lower the central pressure, the greater the pressure gradient between the central and surrounding areas, resulting in higher wind speeds near the center [30]. Therefore, typhoon intensity serves as a fundamental factor influencing wind speed at the wind measurement tower.

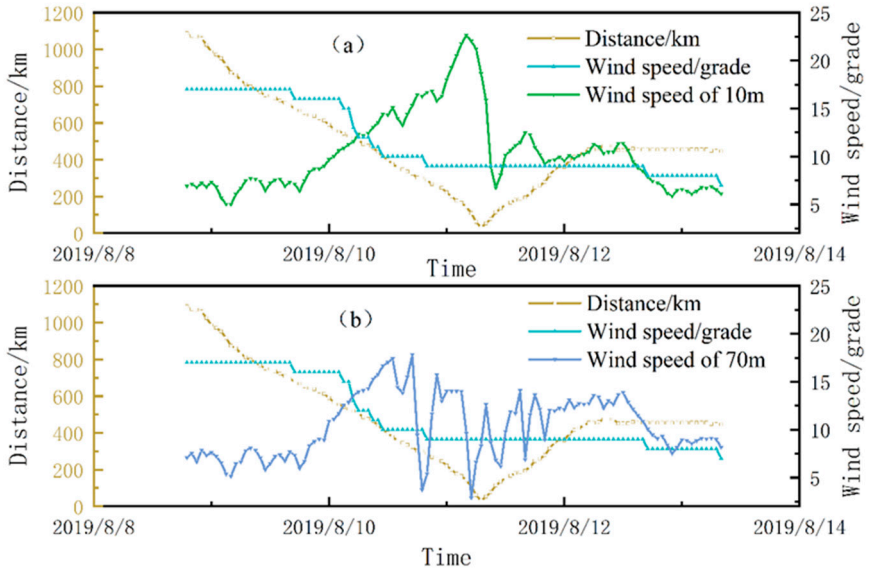

Figure 5. Influence of the cushion on the wind speed of the tower (**a**,**b**).

In this study, hourly wind speed data at the tower were recorded from the onset of typhoon influence until its dissipation. The analysis focused on wind speed near the typhoon center and the distance between the typhoon and the tower. Figure 5 illustrates the impact of the distance between the typhoon center and the wind tower, and the wind level near the typhoon center, on wind speed at the tower. Before landfall, Typhoon Lekima affected the tower's wind speed despite not yet making landfall in Wenling, Zhejiang Province. The typhoon center was located at 125.10° E, 24.30° N, approximately 1088 km from the tower. The minimum central pressure was 920 hPa, with a maximum wind speed near the center of 58 m/s. By 7:00 on 11 August 2019, as the typhoon passed directly over the tower, its center was just 30 km away, with a minimum central pressure of 982 hPa and a maximum wind speed near the center of 23 m/s. Even after the typhoon ceased numbering on 13 August 2019, its circulation continued to influence wind speeds at the tower. At this point, the center was positioned at 119.90° E, 37.50° N, approximately 446 km from the tower, with a minimum central pressure of 990 hPa and a maximum wind speed near the center of 16 m/s.

During the observation period, hourly wind speeds at 10 m showed a significant negative correlation with the distance between the typhoon center and the tower ($p < 0.05$, $R^2 = 0.85$), as well as with wind intensity ($p < 0.05$, $R^2 = 0.88$), indicating continued influence from the typhoon's circulation. As the typhoon center gradually moved northward, wind speeds at the tower steadily increased due to the expanding radius of the typhoon. A significant negative correlation was observed between 10 m wind speed and the distance from the tower to the typhoon center ($p < 0.05$, $R^2 = 0.09$), as well as with wind intensity ($p < 0.05$, $R^2 = 0.69$). However, as the typhoon's radius diminished, wind speed at the tower became primarily influenced by local wind conditions rather than the typhoon's circulation.

In contrast, wind speed at 70 m exhibited greater volatility. It gradually increased before the typhoon's passage, peaking at 17 m/s around 13:00 on 10 August 2019. Subsequently, wind speed fluctuated before stabilizing. Prior to the typhoon's passage, hourly wind speed at 70 m demonstrated a significant negative correlation with the distance from the typhoon to the tower ($p < 0.05$, $R^2 = 0.23$), as well as with wind intensity ($p < 0.05$, $R^2 = 0.33$). However, post-typhoon, wind speed at 70 m showed no significant correlation with the distance to the typhoon ($p = 0.31$, $R^2 = 0.001$), while remaining significantly correlated with wind intensity ($p < 0.05$, $R^2 = 0.33$).

Compared to wind speed at 10 m, wind speed at 70 m exhibited weaker correlations with both the distance from the typhoon and wind intensity, both before and after its passage. This indicates that there may be external factors influencing wind speed at this height.

4.5. Influence of the Cushion on the Wind Speed of the Tower

Terrain and surface type significantly impact the intensity and trajectory of typhoons, subsequently influencing the extreme wind speeds and duration experienced by station wind towers [31]. Examining the path of Typhoon "Likema," it traversed primarily through Zhejiang, Jiangsu, and Shandong provinces. As shown in Figure 6a, analyzing the terrain of these regions reveals distinct characteristics. Zhejiang's topography slopes from southwest to northeast, with mountainous terrain dominating the southwest and alluvial plains in the northeast. Notably, mountain ridges such as Dappan Mountain, Tiantai Mountain, Kuangcang Mountain, and Kuaiji Mountain align in the southwest to northeast direction, with peak elevations ranging from 1100 m to 1400 m. After making landfall in Wenling, Zhejiang Province, the typhoon veered northwestward, reaching the northern Zhejiang Plain within 12 h. During this period, the central wind velocity decreased from 52 m/s at landfall to 28 m/s, and the typhoon's trajectory shifted from northwest to north. While wind speeds at 10 m height continued to rise, those at 70 m displayed a temporary weakening trend, dropping from 17 m/s to 3 m/s. Additionally, wind direction fluctuations were observed at both heights, with a notable 100° larger reduction in wind direction at 70 m compared to 10 m.

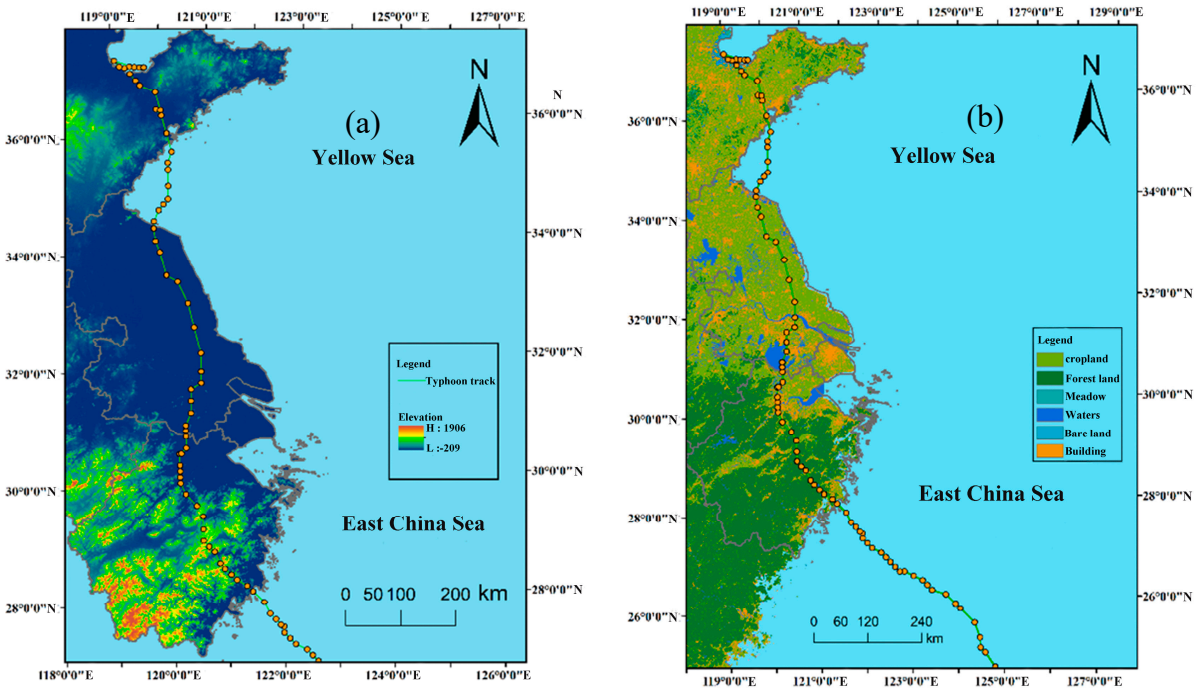

Figure 6. Typhoon track area topography and surface type (**a**,**b**).

Jiangsu, characterized by flat terrain and low average altitude, experiences a different influence from the typhoon's passage. As the typhoon moves across the northern Zhejiang Plain towards the wind tower, it traverses through the middle and lower Yangtze River Plain and the North China Plain. During this phase, spanning a linear distance of approximately 350 km, the central wind speed reduces to 23 m/s and maintains this speed before reaching the wind measurement tower after 15 h. Interestingly, while wind speeds at 10 m height continued to increase, those at 70 m height exhibited a rising-then-decreasing pattern. Similarly, wind direction at both heights showed fluctuations, with a period of low direction at 70 m. This suggests that typhoons advance more swiftly through mountainous regions with complex terrain compared to plain areas, with stronger restraining effects near their centers. Wind speeds and directions at 70 m height are more influenced by large-scale typhoon circulation compared to those at 10 m height.

As shown in Figure 6a, Analyzing surface type distribution in the typhoon's transit area reveals high forest coverage in Zhejiang's mountainous regions, while the northern Zhejiang Plain and Jiangsu Plain are characterized by water systems, urban agglomerations, and farmlands. In urbanized areas like southern Jiangsu, wind tower wind speeds and directions undergo significant changes, with wind speeds at 70 m height dropping to as low as 3 m/s and wind direction shifting from 112° to 90°. This underscores the substantial influence of surface type on high-altitude wind speed and direction, emphasizing the lesser impact of large-scale typhoon circulation on near-surface wind characteristics.

4.6. Influence of Mesoscale System on Wind Speed of Measuring Tower before and after Typhoon

To delve into the discrepancies in wind speed and direction variation between altitudes of 10 m and 70 m, further analysis was conducted on the mesoscale system characteristics before and after typhoon transit, utilizing NCEP reanalysis data at a 2.5° × 2.5° resolution four times a day. Focusing on the distribution of meridional (north-south) and zonal (east-west) winds (U and V) near the latitude and longitude (120° E, 33° N) of the wind tower, several key findings emerged [32].

As is shown in Figure 7, Before the typhoon transit, the east–west and north–south components of Typhoon Lekima" were balanced. Specifically, the wind measuring tower experienced influence from the easterly wind region, concentrated predominantly in the southern portion of 33° N. This easterly wind zone spanned from 600 hPa to 900 hPa and 25° N to 30° N in the atmosphere, and from 400 hPa to 1000 hPa and 30° N to 35° N at the latitude of 33° N. Notably, the position of the strong northerly wind region was comparatively lower, featuring a more stable pressure field than the easterly wind region. This stability resulted in stronger airflow disturbance at various altitude levels within the easterly wind region. Consequently, the wind direction at 70 m altitude was stronger and more volatile compared to that at 10 m altitude before the typhoon's passage.

Subsequent to the typhoon's transit, the westerly gale area gradually shifted southward from around 33° N. Within this gale area, wind speeds gradually decreased from 15 m/s to 10 m/s, and its scale expanded from 600 hPa to 1000 hPa down to 400 to 1000 hPa. Additionally, a southerly gale area persisted south of 33° N, maintaining wind speeds at each altitude level within the range of 0–5 m/s. However, the intensity of change in wind speed was smaller compared to the north–south component. Consequently, after the typhoon's passage, the wind direction at 70 m altitude remained larger and more unstable than that at 10 m altitude, as the wind speed experienced greater fluctuations.

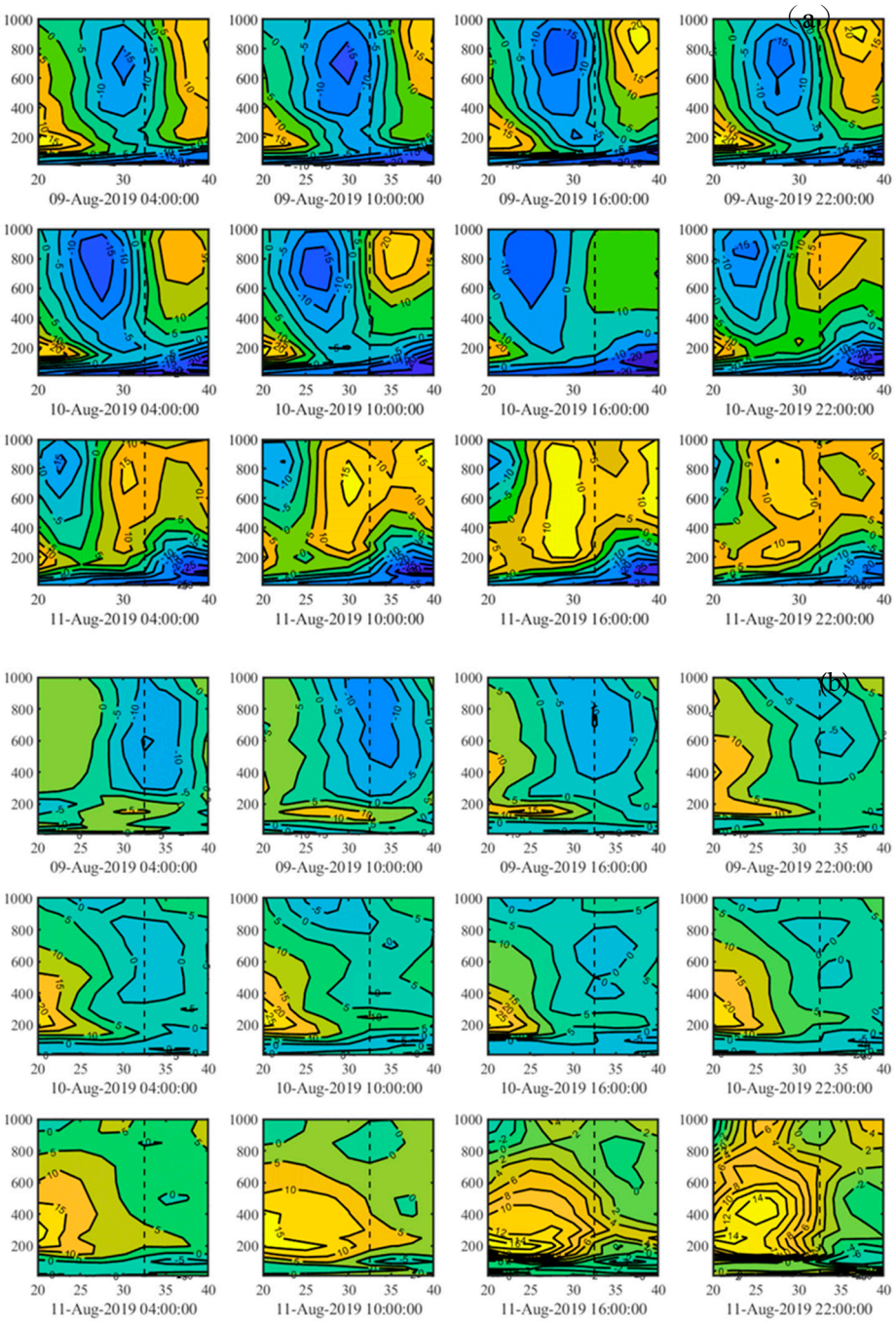

Figure 7. Profile U and V of wind speed near the tower (**a**,**b**).

5. Discussion

5.1. Comparison of BEAST Method with MK and BFAST

Wind speed data at 10 m altitude underwent MK mutation testing and BFAST change point detection to delineate trend and seasonal variations in the time series data [33,34]. The MK mutation test, a non-parametric statistical method, was employed to detect changes in wind speed without imposing distributional assumptions on the samples [33]. Meanwhile, the BFAST method decomposed the time series into trend, seasonal, and residual components, subsequently identifying change points within the trend and seasonal components [34]. Figure 8 illustrates the outcomes of trend change detection using the MK and BFAST methods.

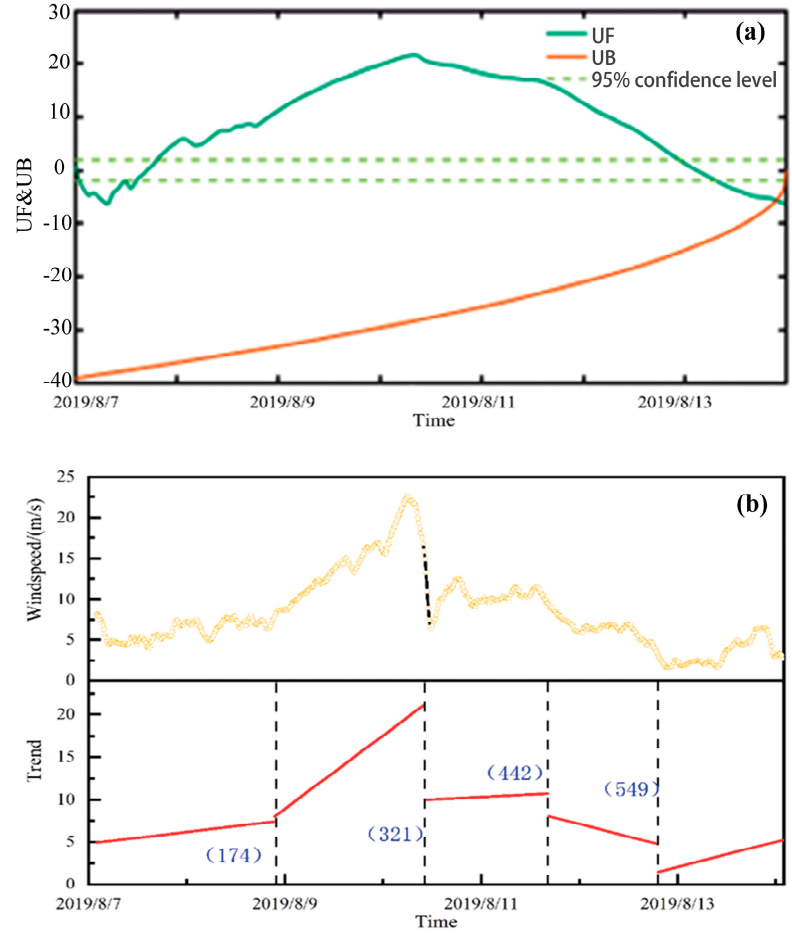

Figure 8. MK and BFAST change detection methods (**a**,**b**).

The results from the MK mutation test revealed that from 8 August at 5:00 to 14 August at 2:30, the UF (U statistic) value consistently exceeded 0, indicating a sustained upward trend in wind speed at 10 m altitude. Although the UF and UF curves intersected at 21:45 on 14 August, they failed to meet the significance level test at 0.05. On the other hand, the BFAST method identified four change points at sequences 174, 321, 442, and 549, respectively. Prior to sequence point 321, two sub-sequences (0–174, 175–321) displayed increasing trends, while sequences 550–672 exhibited an increasing trend, and 322–442 and 443–549 displayed weakening trends. Despite discrepancies in the number and timing of change points between BFAST and BEAST methods, the wind speed series generally depicted both increasing and weakening trends [34].

The MK method, primarily suited for detecting monotonic trends in categorical and sequential variables, may not be suitable for identifying multiple breakpoints [35]. In contrast, the BFAST method utilizes ordinary least squares and minimum sum of squares of residuals (OLS-MOSUM) to pinpoint trend change points, selecting the optimal model based on stable regression detection estimates [36]. On the other hand, the BEAST method, grounded in Bayesian principles, determines the probability value of each sample point's change according to a model space probability distribution, allowing for the detection of subtle change trends [37]. The discrepancy between BFAST and BEAST change points may arise from BEAST's capability to discern nuanced changes. However, the BFAST method requires manual specification of the minimum detection interval factor in parameters, potentially resulting in fewer change points detected compared to the BEAST method [20,38].

5.2. Analysis of the Influence of Typhoon on Wind Farms and Its Measures

Preliminary analysis indicated that during the passage of Typhoon Lekima, wind speeds at the wind farm's 10 m, 30 m, and 50 m heights initially intensified and subsequently weakened, revealing high non-stationarity, particularly at lower altitudes, as indicated by their Hurst indices. However, at 70 m height, wind speed variations were more pronounced, with higher Hurst indices and notable wind direction fluctuations. Given that the wind turbine's hub height is 96 m and rotor diameter is 148 m, the significant wind speed gradients and increased vertical wind shear during typhoons can amplify cyclic fluctuation loads on the turbine, affecting its fatigue performance and shortening its operational lifespan [36]. Sudden shifts in wind direction can also stress turbines equipped with less responsive yaw systems, potentially leading to blade flutter and reduced blade longevity [39].

Over the past decade (2012–2022), Yancheng, Jiangsu Province experienced an average of one typhoon per year, with near-central wind speeds ranging from 16 m/s to 33 m/s. Notably, only the 18th typhoon, "Dawei," in 2012 surpassed 25 m/s wind speeds (Figure 9). Based on Typhoon Lekima's wind speed characteristics, the impact of strong winds and abrupt wind direction changes on wind turbines, and recent typhoon occurrences, the following measures are proposed:

(i) Strengthening Anti-Typhoon and Anti-Gale Early Warning Systems:

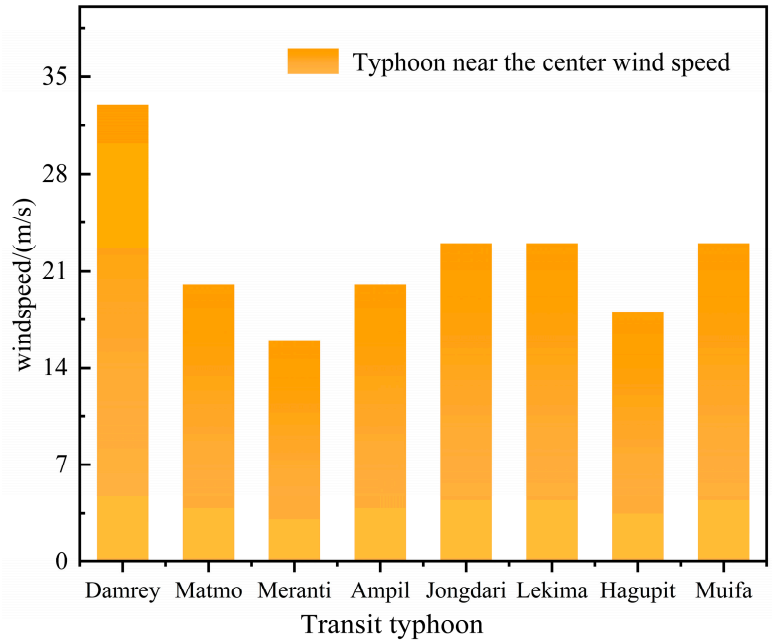

Figure 9. Transit tower typhoon over the years.

Implement an integrated intelligent supervision system across wind farms to enhance data analysis and interoperability, enabling early detection and warning of typhoon paths, wind speeds, and wind directions;

(ii) Enhancing Wind Turbine Control System Upgrades and Maintenance:

Prioritize maintenance and control system upgrades, including variable pitch, yaw, and braking systems, to mitigate typhoon damage [40]. Ensure system operability during typhoons through annual inspections and necessary upgrades;

(iii) Investing in Energy Storage Systems:

Given the region's strong economic development and electricity demand, deploy advanced energy storage technologies to address short-term power supply interruptions

during typhoons [41]. These systems also support long-distance power transmission and contribute to achieving carbon reduction goals.

5.3. Deficiencies and Prospects

Based on the data of wind speed and direction at different heights of the wind tower measured every 15 min, this paper analyzed the change characteristics of wind speed and direction by using BFAST and Hurst index. Meanwhile, based on path characteristics, surface characteristics, and mesoscale wind direction characteristics, it explored the reasons affecting the change characteristics of wind speed and direction. There are the following deficiencies:

(i) Based on the change point, this study artificially divides the wind speed and direction data of the wind tower at different heights into the strengthening stage and weakening stage according to time node 325. Such division may cause the Hurst index and direction characteristic analysis to affect the judgment of the result due to the error of sample data;

(ii) In this study, the distance from the typhoon center to the tower and the effect of the wind speed near the typhoon center on the wind speed of the tower, surface characteristics, and mesoscale wind direction characteristics were selected as the external characteristics that affect the wind speed and wind direction of the wind tower. In the coastal area, SST, sea and land local circulation, and atmospheric circulation were the main factors that affected the wind speed and wind direction [42], which will become the influencing factors for the wind speed change of the wind tower during typhoons in the future.

In extreme weather systems, higher requirements are put forward for the power prediction of wind turbines and the design of wind turbines. In this paper, the characteristics and influencing factors of wind speed and direction change of wind towers in wind farms were studied in order to further study the wind power prediction model in the future.

6. Conclusions

Based on wind speed and wind direction data at 10 m, 30 m, 50 m, and 70 m heights of a wind power tower in Yancheng, Jiangsu Province, this paper analyzed the change characteristics of wind speed and wind direction by using the BFAST method and Hurst index. Based on data on the distance from the typhoon center to the tower and the effect of the wind speed near the typhoon center on the wind speed of the tower, topographic data, and mesoscale system wind direction data, the causes of the occurrence and development of wind speed and wind direction of wind tower were further analyzed, and the conclusions are as follows:

(i) In the BFAST method, there were 5, 5, 6, and 6 change points at the height of 10 m, 30 m, 50 m and 70 m, respectively. Among them, the change points at the height of 10 m, 30 m, and 50 m all changed before and after node 325, while the change time point at the height of 70 m was inconsistent with other heights. Hurst index results showed that the non-stationarity of wind speed series at 70 m altitude was stronger than that at other altitudes;

(ii) The wind direction sequence at the height of 10 m, 30 m, 50 m, and 70 m was fitted by stages. It was found that the direction of wind direction was SE–E–SE–SW–W–NW. Among them, the trend line fitted at the height of 70 m had a large deviation from other altitudes at the wind speed strengthening and weakening stages;

(iii) The wind speed at the heights of 10 m and 70 m had different response degrees to the distance from the typhoon center to the tower and the effect of the wind speed near the typhoon center on the wind speed of the tower. The correlation between the wind speed and the distance between the wind measurement tower and the typhoon near the center was stronger at the height of 10 m than at the height of 70 m. The surface type and the wind direction of the mesoscale system also had certain effects on the wind speed and direction.

In this paper, the change characteristics and influencing factors of wind speed and direction of wind tower were studied, which provides methods and theoretical support for the study of short-term wind speed when a typhoon passes through and provides reliable support for the selection of wind power forecast indicators and the selection and design of wind turbines under extreme gale weather systems.

Author Contributions: Conceptualization, L.W. and A.F.; methodology, L.W.; software, L.W. and J.G.; validation, L.W., H.S. and J.G.; formal analysis, A.F.; investigation, A.F.; resources, L.W., A.F. and J.G.; data curation, H.S.; writing—original draft preparation, L.W., L.D. and W.D.; writing—review and editing, J.G., B.B. and K.A.; visualization, J.G. and K.A.; supervision, K.A.; project administration, L.W.; funding acquisition, B.B. All authors have read and agreed to the published version of the manuscript.

Funding: This work was supported by the New power system technology project of China Southern Power Grid Corporation (000000KK52210138), author Lingzi Wang, and the Second Tibet Plateau Scientific Expedition and Research Program (STEP) under grant number 2019QZKK0804, author Wenzheng Yu. This work also was supported by the Researchers Supporting Project, grant number (RSP2024R296), King Saud University, Riyadh, Saudi Arabia.

Data Availability Statement: The data presented in this study are available upon request from the corresponding authors. The data are not publicly available due to privacy.

Acknowledgments: We would like to thank China Southern Power Grid Company's New Power System Technology Project (000000KK52210138) and the Second Qinghai-Tibet Plateau Scientific Investigation and Research Program (Approval number: 2019QZKK0804) for providing funding for this research, and Jiangsu Haihailongyuan Wind Power Co., Ltd. (Rudong, China) for providing wind speed and direction data. Thank you to everyone who contributed to the study.

Conflicts of Interest: The authors declare that they have no conflicts of interest to report regarding the present study.

References

1. Sahu, B.K. Wind energy developments and policies in China: A short review. *Renew. Sustain. Energy Rev.* **2018**, *81*, 1393–1405. [CrossRef]
2. Chen, Y.; Zhang, D.; Qi, W. Power prediction of a Savonius wind turbine cluster considering wind direction characteristics on three sites. *J. Clean. Prod.* **2023**, *423*, 138789. [CrossRef]
3. Tao, T.; Long, K.; Yang, T. Quantitative assessment on fatigue damage induced by wake effect and yaw misalignment for floating offshore wind turbines. *Ocean Eng.* **2023**, *288*, 116004. [CrossRef]
4. Wang, H.; Wang, T.; Ke, S. Assessing code-based design wind loads for offshore wind turbines in China against typhoons. *Renew. Energy* **2023**, *212*, 669–682. (In Chinese) [CrossRef]
5. Duan, J.; Zhang, L.; Xie, Z.N. Study on non-stationary wind characteristics of mangosteen Typhoon. *J. Vib. Shock* **2022**, *41*, 18–26. (In Chinese)
6. Hui, Y.; Li, B.; Kawai, H. Non-stationary and non-Gaussian characteristics of wind speeds. *Wind Struct.* **2017**, *24*, 59–78. [CrossRef]
7. Qin, Z.Q.; Xia, D.D.; Dai, L.M. Investigations on Wind Characteristics for Typhoon and Monsoon Wind Speeds Based on Both Stationary and Non-Stationary Models. *Atmosphere* **2022**, *13*, 178. [CrossRef]
8. Mahrt, L.; Nilsson, E.; Rutgersson, A. Sea-Surface Stress Driven by Small-Scale Non-stationary Winds. *Bound.-Layer Meteorol.* **2020**, *176*, 13–33. [CrossRef]
9. Chen, C.; Meng, D. Variation characteristics of low altitude wind speed in Wuhan City from 1958 to 2013. *Resour. Environ. Yangtze Basin* **2015**, *24*, 30–37. (In Chinese)
10. Han, L.; Wang, J.P.; Wang, G.Z. Temporal and spatial characteristics of wind speed variation in the wind erosion area of northern China. *Arid Land Geogr.* **2018**, *41*, 963–971. (In Chinese)
11. Xu, J.; Hu, Y.Z.; Li, J.X. Analysis of Long-Term Wind Speed Trends and Assessment of Wind Resources in China Sea Area under the Background of Global Warming. *Adv. Mar. Sci.* 1–12. (In Chinese)
12. Zhao, L.; Wei, C.; Wang, Y. Macro Location of Offshore Wind Farms and Estimation of Wind Energy Resources Reserves. *Acta Energiae Solaris Sin.* 2024; 1–7. (In Chinese)
13. Chen, W.C.; Liu, A.J.; Song, L.L. A case study of wind characteristics of different strong wind weather systems. *Meteorol. Mon.* **2019**, *45*, 251–262. (In Chinese)
14. Wang, H.L.; Wu, X.Q.; Huang, H.Z. Analysis of variation characteristics of near-ground wind speed during the landing of super Typhoon Rammasun. *J. Trop. Meteorol.* **2018**, *34*, 297–304. (In Chinese)

15. Wei, X.W.; Qiu, X.Y.; Li, X.Y. Multi-objective reactive power optimization of power grid including wind farm. *Power Syst. Prot. Control* **2010**, *38*, 107–111. (In Chinese)
16. Jiang, S.; Xu, P.P.; Li, X. Study on the conversion coefficient of wind speed at different elevations and the variation characteristics of wind speed at higher elevations in offshore wind farms. *Power Syst. Big Data* **2022**, *25*, 52–59. (In Chinese)
17. Van Jaarsveldt, C.; Peters, G.W.; Ames, M.; Chantler, M. Tutorial on empirical mode decomposition: Basis decomposition and frequency adaptive graduation in non-stationary time series. *IEEE Access.* **2023**, *11*, 94442–94478. [CrossRef]
18. Jamali, S.; Jönsson, P.; Eklundh, L.; Ardö, J.; Seaquist, J. Detecting changes in vegetation trends using time series segmentation. *Remote Sens. Environ.* **2015**, *156*, 182–195. [CrossRef]
19. Verbesselt, J.; Hyndman, R.; Newnham, G. Detecting trend and seasonal changes in satellite image time series. *Remote Sens. Environ.* **2010**, *114*, 106–115. [CrossRef]
20. Zhao, K.; Wulder, M.A.; Hu, T. Detecting change-point, trend, and seasonality in satellite time series data to track abrupt changes and nonlinear dynamics: A Bayesian ensemble algorithm. *Remote Sens. Environ.* **2019**, *232*, 111181. [CrossRef]
21. Fang, X.; Zhu, Q.; Ren, L. Large-scale detection of vegetation dynamics and their potential drivers using MODIS images and BFAST: A case study in Quebec, Canada. *Remote Sens. Environ.* **2018**, *206*, 391–402. [CrossRef]
22. Dellicour, S.; Gill, M.S.; Faria, N.R. Relax, Keep Walking—A Practical Guide to Continuous Phylogeographic Inference with BEAST. *Mol. Biol. Evol.* **2021**, *38*, 3486–3493.
23. Yuan, Q.Y.; Yang, Y.; Li, C. Research on wind speed time series based on Hurst index. *Appl. Math. Mech.* **2018**, *39*, 798–810. (In Chinese)
24. Xu, Z.F.; Zou, J.H.; Li, C. Hurst index analysis of wind speed time series based on R/S class analysis. *Appl. Math. Mech.* **2019**, *39*, 585–590+604. (In Chinese)
25. Cai, J.Z.; Xu, J.Y.; Shao, X. Analysis of wind field and turbulence characteristics of Typhoon Lekima. *J. Nanjing Univ. (Nat. Sci.)* **2021**, *57*, 896–903. (In Chinese)
26. Sun, Y.W.; Fu, D.; Wang, B. Cause analysis of precipitation caused by Typhoon "Lekima" in Shandong Province. *Trans. Oceanol. Limnol.* **2023**, *45*, 17–22. (In Chinese)
27. Wang, Y.Z.; Li, B.; Wang, R.Q. Application of the Hurst exponent in ecology. *Comput. Math. Appl.* **2011**, *61*, 2129–2131.
28. Gao, Y.; Zhang, Y.; Lei, L.; Tang, J. Multi-scale characteristics of an extreme rain event in Shandong Province, produced by Typhoon Lekima (2019). *Front. Earth Sci.* **2023**, *10*, 1093545.
29. Li, X.X.; Zhang, Y.X.; Cao, X.Z. Analysis of SST variation characteristics of Typhoon Lekima (1909). *Chin. J. Atmos. Sci.* **2023**, *47*, 1295–1308. (In Chinese)
30. Lin, Q.H.; Ding, S. Analysis of Typhoon-Induced Wind Fields in Ports of the Central and Northern Taiwan Strait. *Sustainability* **2024**, *16*, 167.
31. Petrovic, P.; Romanic, D.; Curic, M. Homogeneity analysis of wind data from 213 m high Cabauw tower. *Int. J. Climatol.* **2018**, *38*, E1076–E1090.
32. Huang, W.F.; Xu, Y.L.; Li, C.W. Prediction of design typhoon wind speeds and profiles using refined typhoon wind field model. *Adv. Steel Constr.* **2011**, *7*, 387–402.
33. Zhang, C.Y.; Peng, L. Analysis on variation characteristics of wind direction and speed in Hongjia meteorological Station from 1981 to 2010. *J. Meteorol. Res. Appl.* **2017**, *38*, 72–76+115. (In Chinese)
34. Hu, D. GPS Time Series Is Analyzed by BFAST Algorithm. Ph.D. Thesis, Southwest Jiaotong University, Chengdu, China, 2017.
35. Liu, X.W.; Xu, Z.X. Spatial and temporal pattern of extreme temperature during 1961–2018 in China. *J. Water Clim. Change* **2020**, *11*, 1633–1644.
36. Mendes, M.P.; Rodriguez-Galiano, V.; Aragones, D. Evaluating the BFAST method to detect and characterise changing trends in water time series: A case study on the impact of droughts on the Mediterranean climate. *Sci. Total Environ.* **2022**, *846*, 157428. [CrossRef] [PubMed]
37. Gill, M.S.; Lemey, P.; Suchard, M.A. Online Bayesian Phylodynamic Inference in BEAST with Application to Epidemic Reconstruction. *Mol. Biol. Evol.* **2020**, *37*, 1832–1842. [PubMed]
38. Lyu, R.; Pang, J.; Zhang, J.; Zhang, J. The impacts of disturbances on mountain ecosystem services: Insights from BEAST and Bayesian network. *Appl. Geogr.* **2024**, *162*, 103143. [CrossRef]
39. He, G.L.; Tian, J.K.; Chang, D.S. Typhoon resistance concept design of offshore wind turbine. *Electr. Power Constr.* **2013**, *34*, 11–17. (In Chinese)
40. Liu, J.; Zhang, Z.Q.; Gan, Q.Y. Optimal control of independent variable pitch of wind turbine based on random disturbance correction. *Control. Theory Appl.* 2024; 1–7. (In Chinese)
41. Tang, J.; Yue, F.; Wang, L.X. Global new energy storage technology development situation analysis. *J. Glob. Energy Interconnect.* **2024**, *7*, 228–240. (In Chinese)
42. Qiu, X.N.; Fan, S.J. Application of the data of automatic weather station in the study of local circulation such as sea and land winds. *Acta Sci. Nat. Univ. Sunyatseni* **2013**, *52*, 133–136. (In Chinese)